A global perspective on CMIP5 climate model biases

Article *in* Nature Climate Change · February 2014

DOI: 10.1038/nclimate2118

CITATIONS
328

READS
1,062

5 authors, including:

Chunzai Wang
Chinese Academy of Sciences
174 PUBLICATIONS **8,169** CITATIONS
SEE PROFILE

Liping Zhang
GFDL/NOAA
40 PUBLICATIONS **1,529** CITATIONS
SEE PROFILE

Sang-Ki Lee
National Oceanic and Atmospheric Administration
98 PUBLICATIONS **3,419** CITATIONS
SEE PROFILE

Lixin Wu
Qingdao National Laboratory for Marine Science and Technology (QNLM)
199 PUBLICATIONS **7,048** CITATIONS
SEE PROFILE

nature climate change

LETTERS

PUBLISHED ONLINE: 23 FEBRUARY 2014 | DOI: 10.1038/NCLIMATE2118

A global perspective on CMIP5 climate model biases

Chunzai Wang[1]*, Liping Zhang [1,2], Sang-Ki Lee[1,2], Lixin Wu[3] and Carlos R. Mechoso[4]

The Intergovernmental Panel on Climate Change's Fifth Assessment Report largely depends on simulations, predictions and projections by climate models[1]. Most models, however, have deficiencies and biases that raise large uncertainties in their products. Over the past several decades, a tremendous effort has been made to improve model performance in the simulation of special regions and aspects of the climate system[2–4]. Here we show that biases or errors in special regions can be linked with others at far away locations. We find in 22 climate models that regional sea surface temperature (SST) biases are commonly linked with the Atlantic meridional overturning circulation (AMOC), which is characterized by the northward flow in the upper ocean and returning southward flow in the deep ocean. A simulated weak AMOC is associated with cold biases in the entire Northern Hemisphere with an atmospheric pattern that resembles the Northern Hemisphere annular mode. The AMOC weakening is also associated with a strengthening of Antarctic Bottom Water formation and warm SST biases in the Southern Ocean. It is also shown that cold biases in the tropical North Atlantic and West African/Indian monsoon regions during the warm season in the Northern Hemisphere have interhemispheric links with warm SST biases in the tropical southeastern Pacific and Atlantic, respectively. The results suggest that improving the simulation of regional processes may not suffice for overall better model performance, as the effects of remote biases may override them.

The United Nations Intergovernmental Panel on Climate Change's Fifth Assessment Report updates the knowledge and understanding of the scientific, technical and socio-economic aspects of climate change. The report relies heavily on the products of climate models. These, however, have serious systematic errors that challenge the reliability of climate predictions. Hence, climate model bias identification and reduction are topics of great importance. One major reason for such biases is the misrepresentations of physical processes, which can be amplified by feedbacks among climate components especially in the tropics. Much effort, therefore, is dedicated to the better representation of physical processes in coordination with intense process studies[5]. This paper focuses on the SST simulations by 22 participants in the Coupled Model Intercomparison Project phase 5 (CMIP5; Supplementary Information). We target the global connections among regional SST biases. The existence of such connections means that efforts to improve model performance cannot be narrowly focused on particular regions.

SSTs simulated by CMIP5 models generally show too low values in the Northern Hemisphere and too high values in the Southern Hemisphere. Annual-mean SST error (that is, mean SST bias for the period from 1900 to 2005) magnitudes can be several degrees Celsius (Fig. 1a). SSTs are clearly too high in the tropical southeastern Pacific and Atlantic and too low in the equatorial and tropical southwestern Pacific. In general, these biases have patterns that are largely independent of season, but amplitudes can vary with season (Supplementary Fig. 1). For example, the warm SST bias in the Southern Ocean is present throughout the year but is much stronger during the austral summer and autumn. It is noted that the SST biases in these models are quite stable during the 1900–2005 period and the models do not show a significant SST bias trend.

The misrepresentation of local processes and/or ocean–atmosphere interactions has caused some of the biases. The too warm SSTs in the tropical southeastern Pacific and Atlantic, for example, have been linked to excessive heat flux into the ocean under insufficient coverage by stratocumulus clouds[6,7] combined with insufficient cooling by ocean transients from the upwelling regions along the eastern coasts[8]. The cold SST bias in the equatorial and tropical southwestern Pacific has been associated with an excessive westward extension of the cold tongue from the eastern equatorial Pacific in association with difficulties in the representation of surface winds and ocean mixing processes[6,9]. A recent study has argued that model biases even far away from the tropics can be linked to those in the tropics[10]. According to the study, cloud errors over the Southern Ocean may be responsible for the generation of a spurious intertropical convergence zone south of the Equator in most CMIP5 models.

We start by investigating the relationships in the global domain between biases in simulated SST and in other features of atmosphere and ocean circulations. For this we take the mean AMOC as reference. The AMOC, which is characterized by warmer and saltier water flowing northward in the upper Atlantic Ocean and by cooler and fresher water flowing southward in the deep ocean[11,12], is crucial to the northward heat transport by the ocean circulation[13–16]. As the first step in our analysis, we perform an inter-model singular value decomposition (SVD) analysis of the SST biases and AMOC streamfunction. The spatial pattern of the first SVD mode of the SST biases in Fig. 1b closely resembles the mean model biases in Fig. 1a. The corresponding AMOC mode is weakened, as indicated by the negative values of the AMOC streamfunction in the upper 3,000 m (Fig. 1c). The time series of the first SVD coefficients are highly and positively correlated (correlation coefficient 0.70). Global SST biases, therefore, strengthen as the AMOC circulation weakens.

We next turn to the SST biases in the North Atlantic and Pacific oceans. It has been shown that a weakening of the AMOC is accompanied by a cooling of the North Atlantic Ocean, whereas a

[1]NOAA Atlantic Oceanographic and Meteorological Laboratory, Miami, Florida 33149, USA, [2]Cooperative Institute for Marine and Atmospheric Studies, University of Miami, Miami, Florida 33149, USA, [3]Physical Oceanography Laboratory/Qingdao Collaborative Innovation Center for Marine Science and Technology, Ocean University of China, Qingdao 266100, China, [4]University of California, Los Angeles, California 90095, USA.
*e-mail: Chunzai.Wang@noaa.gov; ocean.climate.ping@gmail.com

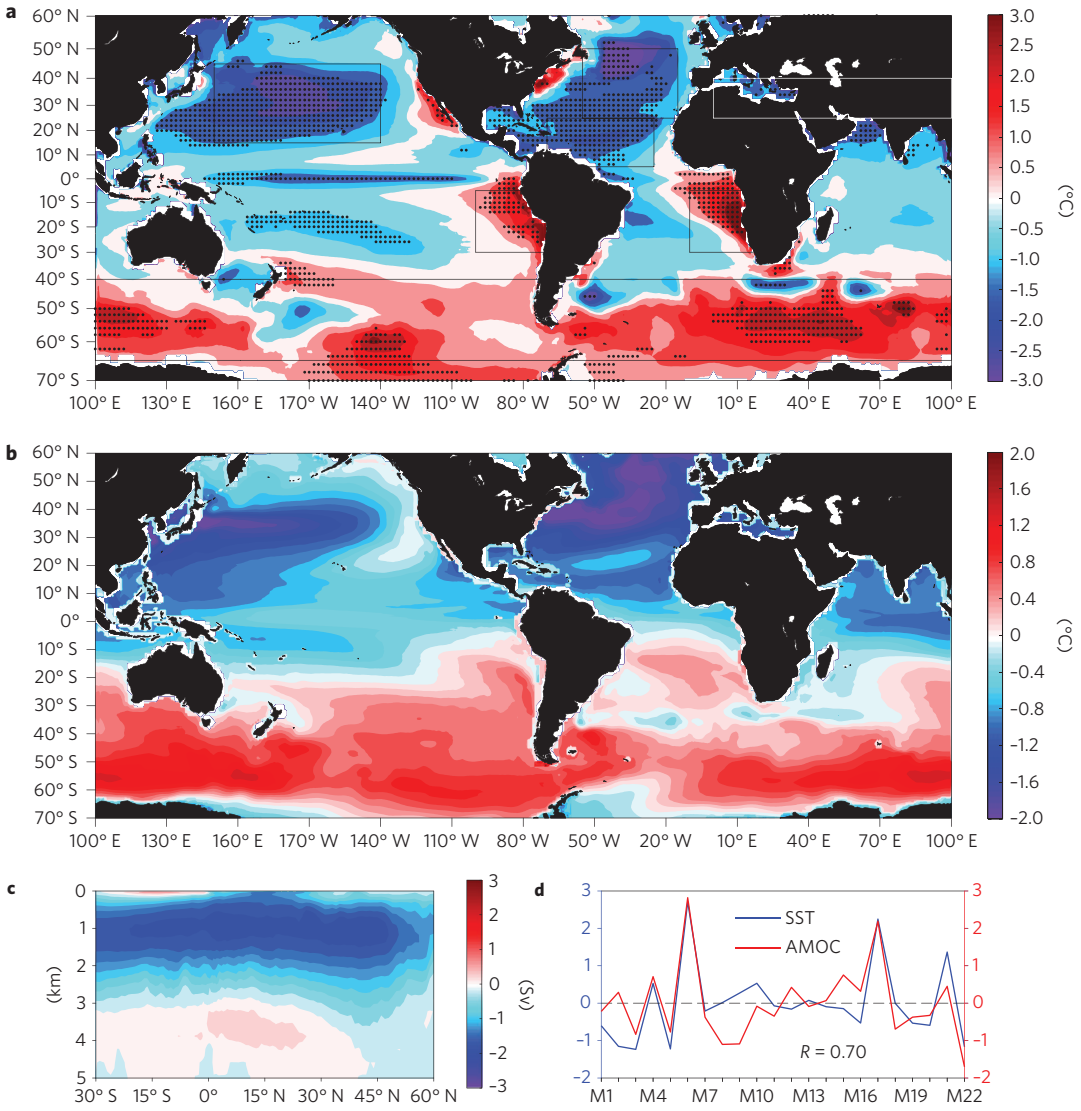

Figure 1 | Global SST bias and its relationship with the AMOC. a, The annual-mean SST bias averaged in 22 climate models. The SST bias is calculated by the SST difference between the model SST and extended reconstructed SST. The dots denote where at least 18 of 22 models (82%) have the same sign in the SST bias. The rectangles represent the focused regions. **b**,**c**, Spatial maps of SST bias and the AMOC for the first inter-model SVD mode (accounting for 45% of total covariance). **d**, Their corresponding coefficients. The *x* axis in **d** represents different models (Supplementary Table 1). The coefficients have been normalized by their own standard deviations.

strengthening is accompanied by a warming of that region[13–16]. This feature is consistently found in the results of water hosing experiments in which an artificial freshening of the subpolar North Atlantic was prescribed in several climate models[17,18]. For quantification, we define an AMOC index as the maximum value of its streamfunction in the latitude band 20° N-60° N. According to Fig. 2a, in 22 CMIP5 models analysed the cold SST bias in the North Atlantic is stronger when the AMOC is weaker, and vice versa, with an inter-model correlation of 0.85 between the SST bias and the AMOC index.

In the North Pacific, the simulated SST biases seem to be linked to those in the North Atlantic (see Fig. 2b). This relationship is primarily a linear one, with an inter-model correlation of 0.61. The correlation coefficient is the highest during the boreal winter and the lowest during the summer (Supplementary Fig. 2). For a better understanding of the links between the SST biases in the North Atlantic and North Pacific, we carry out an inter-model empirical orthogonal function (EOF) analysis of the SST biases. The first EOF mode (EOF1) shows the same sign in the two ocean basins, that is, a cold North Atlantic Ocean corresponds to a cold North Pacific Ocean (Supplementary Fig. 3), and its principal component (PC1) is strongly and negatively correlated with the AMOC index (correlation coefficient −0.85). The pattern of regressions onto PC1 of geopotential height at 200-hPa, sea level pressure and surface wind stress (Supplementary Fig. 4) resembles the Northern Hemisphere annular mode[19], showing that negative sea level pressure anomalies in the North Atlantic correspond to a deepening of the Aleutian low and an intensification of the surface westerly winds in the North Pacific. The intensified westerly winds cool the North Pacific Ocean through enhanced latent heat flux and southward ocean advection associated with Ekman transport. This teleconnection is consistent with previous studies on the impact of the North Atlantic variability on that in the North Pacific[20].

Our next concern is the SST biases in the Southern Ocean. In association with the AMOC, two principal water masses circulate in the deep ocean. One is North Atlantic Deep Water (NADW), which forms in the Nordic, Labrador and Irminger seas owing to atmospheric cooling of salty surface water. The other water

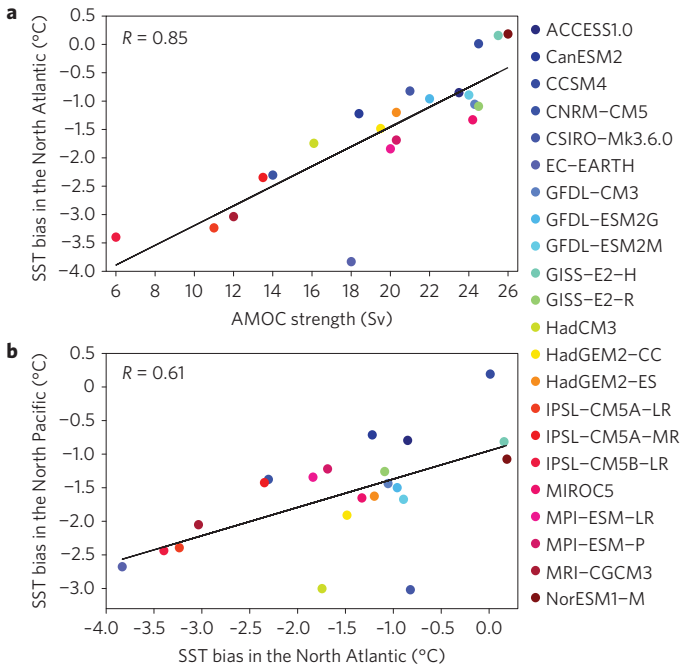

Figure 2 | Relationships of SST bias in the North Atlantic with the AMOC and SST bias in the North Pacific.a, Scatter plot of annual-mean SST bias in the North Atlantic (55° W–15° W, 25° N–50° N) versus AMOC strength. **b**, Scatter plot of annual-mean SST bias in the North Pacific (150°E–140°W, 15° N–45° N) versus the annual-mean SST bias in the North Atlantic. The inter-model correlation *R* is shown in the left-upper side of each panel.

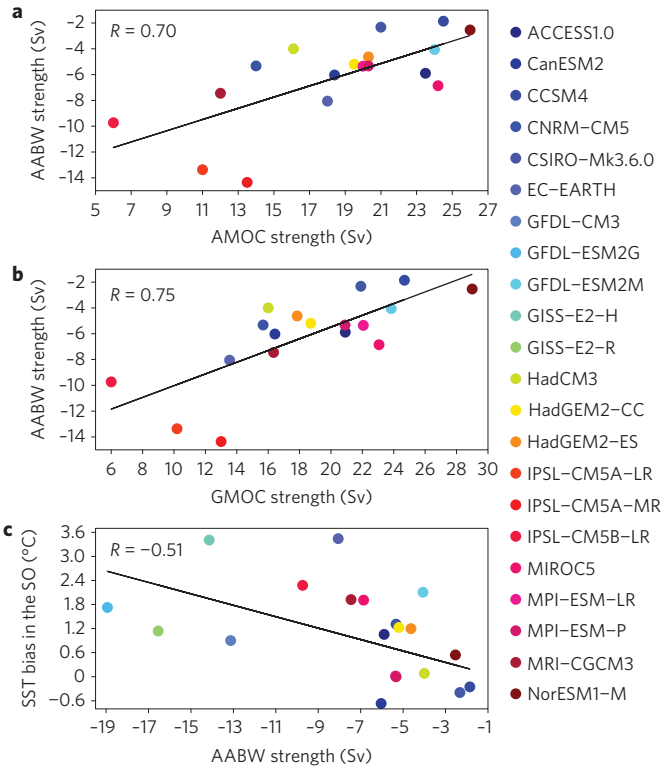

Figure 3 | Relationships of ocean circulation with the warm SST bias in the Southern Ocean.a, Scatter plot of the AMOC versus AABW strength. **b**, Scatter plot of the GMOC versus AABW strength. **c**, Scatter plot of SST bias in the Southern Ocean (SO; 100° E–100° E, 40° S–65° S) versus the AABW strength. The AABW strength is defined as the minimum of the global meridional streamfunction between 60° S–80° S. The inter-model correlation *R* is shown in the left-upper side of each panel.

mass is the Antarctic Bottom Water (AABW), which forms in the Weddell and Ross seas around Antarctica, sinks in the Southern Ocean and flows northward as dense bottom water (Supplementary Fig. 5). The AABW index is defined by the minimum of the global meridional overturning circulation (GMOC) streamfunction between 60° S–80° S (Supplementary Fig. 6)[21]. The simulations by 22 CMIP5 models show an inverse relationship between the AMOC and AABW indices (Fig. 3a). That is, a reduced AMOC is associated with a stronger AABW; the converse is true for an enhanced AMOC. This relationship also holds for the GMOC (Fig. 3b). An explanation of this relationship is that a reduction in the density of NADW associated with a weakened AMOC[22] allows dense surface water in the Southern Ocean to penetrate into the deep sea (that is, an enhanced convection in the Southern Ocean)[23,24]. The enhanced convection is associated with increased convective mixing in the Southern Ocean, which favours a local surface warming (Fig. 3c) because the subsurface ocean is warmer than the surface ocean in the Southern Ocean (Supplementary Fig. 7).

Again we carry out an inter-model EOF analysis of the SST bias, this time for the Southern Hemisphere values. EOF1 shows positive values in the Southern Ocean, and PC1 is negatively correlated with the AABW index (Supplementary Fig. 8). Hence, a warm SST bias in the Southern Ocean corresponds to a stronger AABW as shown in Fig. 3c. Regressions of this PC1 onto the geopotential height at 200-hPa, sea level pressure and surface wind stress fields in the Southern Ocean reveal that higher sea level pressures in the Southern Ocean are associated with surface easterly wind anomalies (a reduction of the westerly winds; Supplementary Fig. 9). The weaker westerly winds are consistent with reduced northward Ekman transport and decreased surface latent heat flux, both of which tend to warm the ocean surface. Local ocean–atmosphere interactions can further amplify the warm SST biases in the Southern Ocean: the westerly wind weakening results in further SST increases[25]. The SST–wind feedback is well represented in the SST and zonal wind stress biases in 22 CMIP5 climate models (Supplementary Fig. 10).

Finally, we turn to the tropical portion of the global SST bias in Fig. 1a. This may be influenced by the SST bias in the higher latitudes[10,26]. For instance, the cloud bias over the Southern Ocean may affect the subtropical atmospheric jet in the Southern Hemisphere to reduce the poleward eddy energy transport and thus warm the tropics[10]. Similarly, the cold SST bias in high latitudes of the Northern Hemisphere can cool the tropics through increased poleward eddy energy transport and the thermal advection and mixing by the westerly wind and eddy in the atmosphere[26]. Our emphasis in this paper is on remote interhemispheric links of the tropical SST biases. In the Western Hemisphere during the summer season, there is strong diabatic heating and ascent over the Atlantic warm pool, which comprises the Gulf of Mexico, Caribbean Sea and western tropical North Atlantic[27]. On seasonal and longer timescales, anomalies in warm pool extent and intensity are associated with changes in the regional ascent and associated descent above the tropical southeastern Pacific in a Hadley-type, interhemispheric circulation[28]. This regional Hadley circulation is stronger during the boreal summer and autumn[27,28]. Consequently, SST biases in the tropical North Atlantic can be linked to those in the tropical southeastern Pacific. As the AMOC weakens, the SST bias in the tropical North Atlantic is cold (Fig. 1), which is associated with the warm SST bias in the tropical southeastern Pacific. The relationship between these SST biases is well represented in

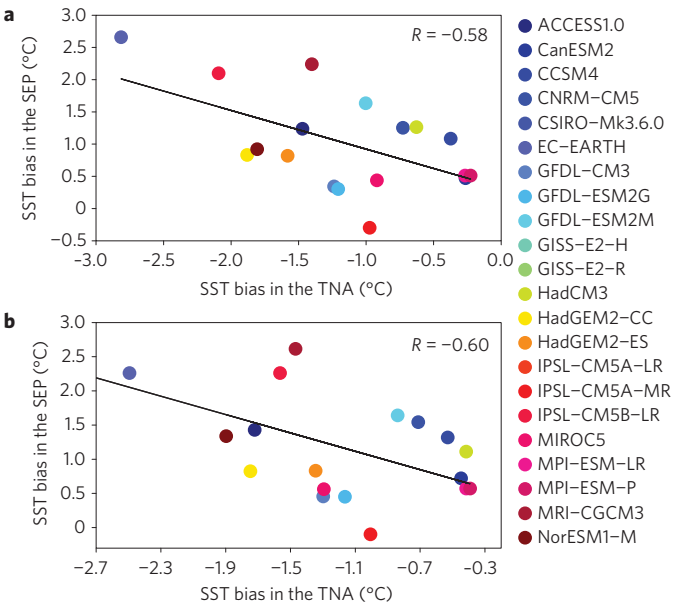

Figure 4 | Interhemispheric link between SST biases in the tropical southeastern Pacific and the tropical North Atlantic.a,**b**, Scatter plots of the SST bias in the tropical southeastern Pacific (SEP) versus the SST bias in the tropical North Atlantic (TNA) during summer (June–August; **a**) and autumn (September–November; **b**). The inter-model correlation *R* is shown in the right-upper side of each panel.

the boreal summer and autumn (Fig. 4). In other seasons, the connection is relatively low (Supplementary Fig. 11).

Interhemispheric links of the biases in the southeastern tropical Atlantic are more challenging to demonstrate. Such interhemispheric connection is plausible because ascent in the monsoon areas of the West African, India and Asian monsoons influences subsidence above the surface anticyclone in the South Atlantic[29]. As discussed earlier in this paper, a weakened AMOC is associated with a cooling of the entire Northern Hemisphere (Fig. 1). The resulting reduction of surface air temperature is consistent with weaker West African and Indian monsoons and with warmer SSTs in the tropical southeastern Atlantic. These relationships also vary with season (Supplementary Fig. 12). The correlations are significant but relatively weak, with the stronger occurring in the boreal summer, when the West African and Indian monsoons are at their peak intensity.

Most state-of-the-art climate models suffer from large and common biases in simulating global SSTs. We have looked at these biases from a global perspective although it is recognized that in regional scales the biases in individual models may depend on different processes. We have linked the SST biases for different regions to the simulated AMOC. This has important practical outcomes and implications. First, improving climate models cannot be reduced to improved representation of regional processes. Second, much is to be done for a better understanding of the global teleconnections that ultimately affect climate model performance. Third, an improvement of the simulated AMOC in climate models is needed for better climate predictions and projections. It is also worth noting that the models with stronger than observed AMOC strength still have cold SST bias in the North Atlantic (Fig. 2a). This suggests that the AMOC strength may not be the only factor that causes the cold SST bias. In particular, it is important to realize that although the AMOC strength is correctly simulated, if the AMOC cell is too shallow, the associated northward heat transport could be too weak. This argument is readily supported by a well-known deficiency in level coordinate models that NADW is too shallow[30]. Further studies are needed to address whether the vertical structure of the AMOC is an important factor that affects the cold SST bias in the North Atlantic.

Received 28 June 2013; accepted 6 January 2014; published online 23 February 2014

References

1. Taylor, K. E., Stouffer, R. J. & Meehl, G. A. An overview of CMIP5 and the experiment design. *Bull. Amer. Meteor. Soc.* **93,** 485–498 (2012).
2. Li, G. & Xie, S.-P. Origins of tropical-wide SST biases in CMIP multi-model ensembles. *Geophys. Res. Lett* **39,** L22703 (2012).
3. Guilyardi, E. *et al.* Understanding El Niño in ocean-atmosphere general circulation models: Progress and challenges. *Bull. Amer. Met. Soc.* **90,** 325–340 (2009).
4. Collins, M. *et al.* The impact of global warming on the tropical Pacific and El Niño. *Nature Geosci.* **3,** 391–397 (2010).
5. Mechoso, C. R. *et al.* Ocean-cloud-atmosphere-land interactions in the Southeastern Pacific: The VOCALS Program. *Bull. Am. Met. Soc.* (in the press, 2013).
6. Mechoso, C. R. *et al.* The seasonal cycle over the tropical Pacific in general circulation models. *Mon. Weath. Rev* **123,** 2825–2838 (1995).
7. Huang, B., Hu, Z.-Z. & Jha, B. Evolution of model systematic errors in the tropical Atlantic basin from the NCEP coupled hindcasts. *Clim. Dynam.* **28,** 661–682 (2007).
8. Colas, F., McWilliams, J. C., Capet, X. & Jaison, K. Heat balance and eddies in the Peru–Chile current system. *Clim. Dynam.* **39,** 509–529 (2012).
9. Davey, M. K. *et al.* STOIC: a study of coupled model climatology and variability in tropical ocean regions. *Clim. Dynam.* **18,** 403–420 (2002).
10. Hwang, Y.-T. & Frierson, D. M. W. Link between the double-Intertropical Convergence Zone problem and cloud biases over the Southern Ocean. *Proc. Natl Acad. Sci. USA* http://dx.doi.org/10.1073/pnas.1213302110PNAS (2013).
11. Wunsch, C. & Heimbach, P. Estimated decadal changes in the North Atlantic meridional overturning circulation and heat flux 1993 2004. *J. Phys. Oceanogr.* **36,** 2012–2024 (2006).
12. Zhang, R. Coherent surface-subsurface fingerprint of the Atlantic meridional overturning circulation. *Geophys. Res. Lett.* **35,** L20705 (2008).
13. Knight, J. R., Allan, R. J., Folland, C. K., Vellinga, M. & Mann, M. E. A signature of persistent natural thermohaline circulation cycles in observed climate. *Geophys. Res. Lett* **32,** L20708 (2005).
14. Folland, C. K., Parker, D. E. & Palmer, T. N. Sahel rainfall and worldwide sea temperatures, 1901–85. *Nature* **320,** 602–607 (1986).
15. Delworth, T. L. & Mann, M. E. Observed and simulated multidecadal variability in the Northern Hemisphere. *Clim. Dynam.* **16,** 661–676 (2000).
16. Zhang, R., Delworth, T. L. & Held, I. Can the Atlantic Ocean drive the observed multidecadal variability in Northern Hemisphere mean temperature? *Geophys. Res. Lett* **34,** L02709 (2007).
17. Stouffer, R. *et al.* Investigating the causes of the response of the thermohaline circulation to past and future climate changes. *J. Clim.* **19,** 1365–1387 (2006).
18. Wu, L., Li, C., Yang, C. & Xie, S.-P. Global teleconnections in response to a shutdown of the Atlantic meridional overturning circulation. *J. Clim.* **21,** 3002–3019 (2008).
19. Thompson, D. W. & Wallace, J. M. Annular modes in the extratropical circulation. Part I: Month-to-month variability. *J. Clim.* **13,** 1000–1016 (2000).
20. Zhang, R. & Delworth, T. L. Impact of the Atlantic Multidecadal Oscillation on North Pacific climate variability. *Geophys. Res. Lett.* **34,** L23708 (2007).
21. Meehl, G. A., Hu, A., Arblaster, J., Fasullo, J. & Trenberth, K. E. Externally forced and internally generated decadal climate variability associated with the Interdecadal Pacific Oscillation. *J. Clim.* **26,** 7298–7310 (2013).
22. Zhang, R. *et al.* Sensitivity of the North Atlantic Ocean circulation to an abrupt change in the Nordic Sea overflow in a high resolution global coupled climate model. *J. Geophys. Res.* **116,** C12024 (2011).
23. Broecker, W. S. Paleocean circulation during the last deglaciation: a bipolar seesaw? *Paleoceanography* **13,** 119–121 (1998).
24. Weaver, A. J., Saenko, O. A., Clark, P. U. & Mitrovica, J. X. Meltwater pulse 1A from Antarctic as a trigger of the Bølling-Allerød warm interval. *Science* **299,** 1709–1713 (2003).
25. Ma, H. & Wu, L. Global teleconnections in response to freshening over the Antarctic Ocean. *J. Clim.* **24,** 1071–1088 (2011).
26. Kang, S. M., Held, I. M. & Xie, S.-P. Contrasting the tropical response to zonally asymmetric extratropical and tropical thermal forcing. *Clim. Dynam.* http://dx.doi.org/10.1007/s00382-013-1863-0 (2013).

27. Wang, C., Enfield, D. B., Lee, S.-K. & Landsea, C. W. Influences of the Atlantic warm pool on Western Hemisphere summer rainfall and Atlantic hurricanes. *J. Clim.* **19,** 3011–3028 (2006).
28. Wang, C., Lee, S.-K. & Mechoso, C. R. Inter-hemispheric influence of the Atlantic warm pool on the southeastern Pacific. *J. Clim.* **23,** 404–418 (2010).
29. Richter, I., Mechoso, C. R. & Robertson, A. W. What determines the position and intensity of the South Atlantic anticyclone in austral winter?—An AGCM study. *J. Clim.* **21,** 214–229 (2008).
30. Yeager, S. & Danabasoglu, G. Sensitivity of Atlantic meridional overturning circulation variability to parameterized Nordic Sea overflows in CCSM4. *J. Clim.* **25,** 2077–2103 (2012).

Acknowledgements

R. Lumpkin served as an internal reviewer of the Atlantic Oceanographic and Meteorological Laboratory (AOML). This work was supported by grants from the National Oceanic and Atmospheric Administration (NOAA) Climate Program Office, National Science Foundation, the base funding of NOAA/AOML, China National Global Change Major Research Project (2013CB956201), and China National Science Foundation Key Project (41130859). The findings and conclusions in this report are those of the author(s) and do not necessarily represent the views of the funding agency.

Author contributions

C.W. and L.Z. designed the study. L.Z. made all plots and analyses. C.W. wrote the paper and C.R.M. contributed significantly to the text. All co-authors helped interpret the analyses and also edited the paper.

Additional information

Supplementary information is available in the online version of the paper. Reprints and permissions information is available online at www.nature.com/reprints. Correspondence and requests for materials should be addressed to C.W. or L.Z.

Competing financial interests

The authors declare no competing financial interests.

nature climate change

SUPPLEMENTARY INFORMATION

DOI: 10.1038/NCLIMATE2118

A Global Perspective on CMIP5 Climate Model Biases

Chunzai Wang [1]

Liping Zhang [2&1]

Sang-Ki Lee [2&1]

Lixin Wu [3]

Carlos R. Mechoso [4]

[1] NOAA Atlantic Oceanographic and Meteorological Laboratory

Miami, Florida

[2] Cooperative Institute for Marine and Atmospheric Studies

University of Miami

Miami, Florida

[3] Physical Oceanography Laboratory/Qingdao Collaborative Innovation Center for Marine Science and Technology

Ocean University of China

Qingdao, China

[4] University of California, Los Angeles

Los Angeles, California

Nature Climate Change

Corresponding author address: Dr. Chunzai Wang, NOAA/Atlantic Oceanographic and Meteorological Laboratory, 4301 Rickenbacker Causeway, Miami, FL 33149, USA.
E-mail: Chunzai.Wang@noaa.gov; or Dr. Liping Zhang, E-mail: ocean.climate.ping@gmail.com.

CMIP5 Climate Models

This study is based on twenty-two coupled general circulation models (CGCMs or climate models) outputs of the "historical" simulations provided to the Intergovernmental Panel on Climate Change's Fifth Assessment Report (IPCC-AR5). The model data can be downloaded from the website of the Coupled Model Intercomparison Project phase 5 (CMIP5)[1] (http://cmip-pcmdi.llnl.gov/cmip5/). The historical run is forced by observed atmospheric composition changes which reflect both anthropogenic (greenhouse gases) and natural (volcanic influences, solar forcing, aerosols and emissions of short-lived species and their precursors) sources and, for the first time, including time-evolving land cover. These historical runs cover much of the industrial period from the mid-nineteenth century to the near present and are sometimes referred to as "twentieth century" simulations. The modeling center, country, model name and letter denotation for each model used in this study are shown in Table S1. Because we are interested in large-scale features, unless otherwise specified, all model outputs are interpolated to a 1° latitude by 1° longitude grid. We choose the period 1900-2005 for our calculations and analyses. The model annual (seasonal) SST biases are calculated as the difference between the model and observational SSTs in the annual (seasonal) mean values during the period from 1900 to 2005.

Data Sets

Many observational and reanalysis data sets are used in this study. The first one is the improved extended reconstructed sea surface temperature (ERSST), with a 2° latitude by 2° longitude resolution[2]. The second data set is the atmospheric reanalysis of the 20th Century Reanalysis version 2 (20CRv2), which contains estimates of global tropospheric variability from 1871 to 2010 at 6-hourly interval with a spatial resolution of 2° latitude by 2° longitude[3]. To

compare with and be consistent with climate model outputs, these two data sets are interpolated to a 1° latitude by 1° longitude grid and the data period 1900-2005 is chosen.

The version 2.2.4 of the Simple Ocean Data Assimilation (SODA)[4] is also used in this study. The SODA uses an ocean general circulation model (GCM) to assimilate available temperature and salinity observations. The product is a gridded data set of oceanic variables with monthly values at a 0.5°×0.5° latitude-longitude horizontal resolution and 40 vertical levels (The SODA product is sometimes called observational data). Additionally, the objectively analyzed temperature and salinity version 6.7 at 24 levels in the upper ocean of 1500 m is used[5]. The analysis is based on the World Ocean Database, the global temperature-salinity in the tropical Pacific from IRD/France, and the Centennial in situ Observation Based Estimates (COBE) SST. The Ishii et al. analysis also includes the Argo profiling data in the final several years and the XBT depth bias correction.

Methods

Several statistical methods are used in this study, such as linear correlation and regression. We perform an inter-model singular value decomposition (SVD) analysis of the SST biases and AMOC streamfunction for 22 CMIP5 climate models. The inter-model SVD is similar to the traditional SVD method[6], but with the continuous space-model field instead of the traditional space-time field. Like the traditional space-time SVD, the space-model is decomposed into space and expansion function of model. The two dimensional fields of the SST bias $SST(s,m)$ and AMOC streamfunction $\psi(s,m)$ are expanded into K orthogonal spatial patterns:

$$SST(s,m) = \sum_{k=1}^{K} u_k(s) a_k(m) \qquad (1)$$

$$\psi(s,m) = \sum_{i=1}^{K} v_i(s) b_i(m) , \qquad (2)$$

where *s* and *m* denote space (latitude-longitude) and model, respectively; u_k and v_i are the vectors which give the full spatial structure of the mode of covariance between the SST and AMOC; a_k and b_i are the corresponding SST bias and AMOC coefficients. To study the influence of the AMOC on the SST bias, we project $SST(s,m)$ and $\psi(s,m)$ onto b_i for showing the spatial maps of the SST biases and AMOC streamfunction.

To examine the inter-model diversity of long-term mean SST bias, we also perform an inter-model empirical orthogonal function (EOF) analysis for 22 CMIP5 climate models. The inter-model EOF is also similar to the traditional EOF method[7], but with the continuous space-model field *X(m, s)* instead of the traditional space-time field *X(t, s)*. Here *m*, *s* and *t* denote different models, spatial position and time, respectively. Like the traditional space-time EOF, the space-model *X(m, s)* is decomposed into space *u(s)* and expansion function of model *c(m)*. The inter-model EOF method has been successfully used for the tropical oceans by Li and Xie[8].

AMOC Streamfunction

The streamfunction of the AMOC is calculated from the ocean meridional velocity $v(x,y,z,t)$ of climate model outputs as:

$$\psi_A(y,z,t) = \int_{-H}^{-z} \int_{X_{WEST}}^{X_{EAST}} v(x,y,z,t)\, dx\, dz , \qquad (3)$$

where H is the sea bottom, X_{WEST} is the ocean western boundary in the Atlantic Ocean, and X_{EAST} is the ocean eastern boundary in the Atlantic Ocean. The unit of the AMOC streamfunction ψ_A is the Sverdrup (1 Sv=10^6 $m^3 s^{-1}$). The AMOC index is defined as the

maximum of the AMOC streamfunction in the latitude range 20°N-60°N and below 500 m. The long-term mean AMOC streamfunction from CMIP5 climate models can be found in Wang and Zhang[9].

GMOC Streamfunction

The global meridional overturning circulation (GMOC) streamfunction is integrated over the global ocean in the zonal direction. That is, given the ocean meridional velocity $v(x,y,z,t)$, the GMOC streamfunction is calculated as:

$$\psi_G(y,z,t) = \int_{-H}^{-z} \int_{Global} v(x,y,z,t)\,dx\,dz\,. \qquad (4)$$

In the calculation, all land areas are omitted. The GMOC index is defined as the maximum of global streamfunction in the latitude range 20°N-60°N and below 500 m. The long-term mean GMOC streamfunction from 22 CMIP5 climate models is shown in Fig. S6.

NADW and AABW

The GMOC or AMOC mainly consists of the upper and lower circulation cells (Fig. S6). The upper cell includes a northward flow in the surface, North Atlantic Deep Water (NADW) in high latitude of the North Atlantic, and a southward return flow at deep depth (Fig. S5). NADW forms in the Nordic, Labrador and Irminger Seas due to atmospheric cooling of salty surface water and sinks to greater depth in the Atlantic basin. A strengthening (weakening) of this upper cell is associated with the warming (cooling) of the North Atlantic Ocean[10, 11]. In other words, NADW is positively related to the strength of the GMOC or AMOC and the North Atlantic SST.

The lower circulation cell is called the Antarctic Bottom Water (AABW) cell, which is primarily driven by the dense water formation of AABW. AABW forms in the Weddell and

Ross Seas in the SO from surface water cooling and brine rejection[12]. Due to the increased density, the convection of AABW sinks to the deep ocean in the SO, flows northward, returns southward at deep depth, and upwells to the sea surface of the SO. This lower circulation cell is indicated by negative values of GMOC streamfunction poleward of about 60°S, and negative values below about 3000 m that extend into the Northern Hemisphere (Fig. S6). As done in the other study[13], we define the AABW index as the minimum of the GMOC streamfunction between 60°S and 80°S.

References

1. Taylor, K. E., Stouffer, R. J. & Meehl, G. A. An overview of CMIP5 and the experiment design. *Bull. Amer. Meteor. Soc.* **93**, 485–498 (2012).
2. Smith, T. M. & Reynolds, R. W. Improved extended reconstruction of SST (1854–1997). *J Clim.* **17**, 2466–2477 (2004).
3. Compo, G. P. et al. The Twentieth Century Reanalysis Project. *Quart. J. Roy. Meteor. Soc.* **137**, 1–28 (2011).
4. Carton, J. A. & Giese, B. S. A reanalysis of ocean climate using Simple Ocean Data Assimilation (SODA). *Mon. Wea. Rev.* **136**, 2999–3017 (2008).
5. Ishii, M., Kimoto, M. Sakamoto, K. & Iwasaki, S. I. Steric sea level changes estimated from historical ocean subsurface temperature and salinity analyses. *J. Oceanography.* **62 (2)**, 155-170 (2006).
6. Wallace, J. M., Smith, C. & Bretherton, C. S. Singular value decomposition of wintertime sea surface temperature and 500-mb height anomalies. *J. Clim.* **5**, 561–576 (1992).

7. Jackson, J. E. A User's Guide to Principal Components. Wiley, New York, p. 569 (1991).
8. Li, G. & Xie, S.-P. Origins of tropical-wide SST biases in CMIP multi-model ensembles. *Geophys. Res. Lett.* **39**, L22703, doi:10.1029/2012GL053777 (2012).
9. Wang, C. & Zhang, L. Multidecadal ocean temperature and salinity variability in the tropical North Atlantic: Linking with the AMO, AMOC and subtropical cell. *J. Clim.* **26**, 6137-6162 (2013).
10. Knight, J. R., Allan, R. J., Folland, C. K., Vellinga, M., Mann, M. E. A signature of persistent natural thermohaline circulation cycles in observed climate. *Geophys. Res. Lett.* **32**, L20708. doi:10.1029/2005GL024233 (2005).
11. Dijkstra, H. A., te Raa, L., Schmeits, M. & Gerrits, J. On the physics of the Atlantic multidecadal oscillation. *Ocean Dyn.* **56,** 36-50 (2006).
12. Maqueda, M., Willmott, A. & Biggs, N. Polynya dynamics: A review of observations and modeling. *Rev. Geophys.* **42**, RG1004, doi:10.1029/2002RG000116 (2004).
13. Meehl, G. A., Hu, A., Arblaster, J., Fasullo, J. & Trenberth, K. E. Externally forced and internally generated decadal climate variability associated with the Interdecadal Pacific Oscillation. *J. Clim.* **26**, 7298-7310 (2013).

Table S1. 22 climate models used in this study and their sponsor, country, name and letter denotation.

Sponsor, Country	Model Name	Letter denotation
Commonwealth Scientific and Industrial Research Organisation (CSIRO), Australia	ACCESS1.0	M1
Canadian Center for Climate Modeling and Analysis, Canada	CanESM2	M2
National Center for Atmospheric Research (NCAR), USA	CCSM4	M3
Météo-France/Centre National de Recherches Météorologiques, France	CNRM-CM5	M4
Commonwealth Scientific and Industrial Research Organisation (CSIRO), Australia	CSIRO-Mk3.6.0	M5
European Earth System Model, EU	EC-EARTH	M6
U.S. Department of Commerce/National Oceanic and Atmospheric Administration (NOAA)/Geophysical Fluid Dynamics Laboratory (GFDL), USA	GFDL-CM3	M7
	GFDL-ESM2G	M8
	GFDL-ESM2M	M9
National Aeronautics and Space Administration (NASA)/Goddard Institute for Space Studies (GISS), USA	GISS-E2-H	M10
	GISS-E2-R	M11
Met office Hadley Centre, UK	HadCM3	M12
	HadGEM2-CC	M13
	HadGEM2-ES	M14
Institute Pierre Simon Laplace, France	IPSL-CM5A-LR	M15
	IPSL-CM5A-MR	M16
	IPSL-CM5B-LR	M17
Center for Climate System Research (University of Tokyo), National Institute for Environmental Studies, and Frontier Research Center for Global Change (JAMSTEC), Japan	MIROC5	M18
Max Planck Institute for Meteorology, Germany	MPI-ESM-LR	M19
	MPI-ESM-P	M20
Meteorological Research Institute, Japan	MRI-CGCM3	M21
Norwegian Climate Centre, Norway	NorESM1-M	M22

Supplementary Figures

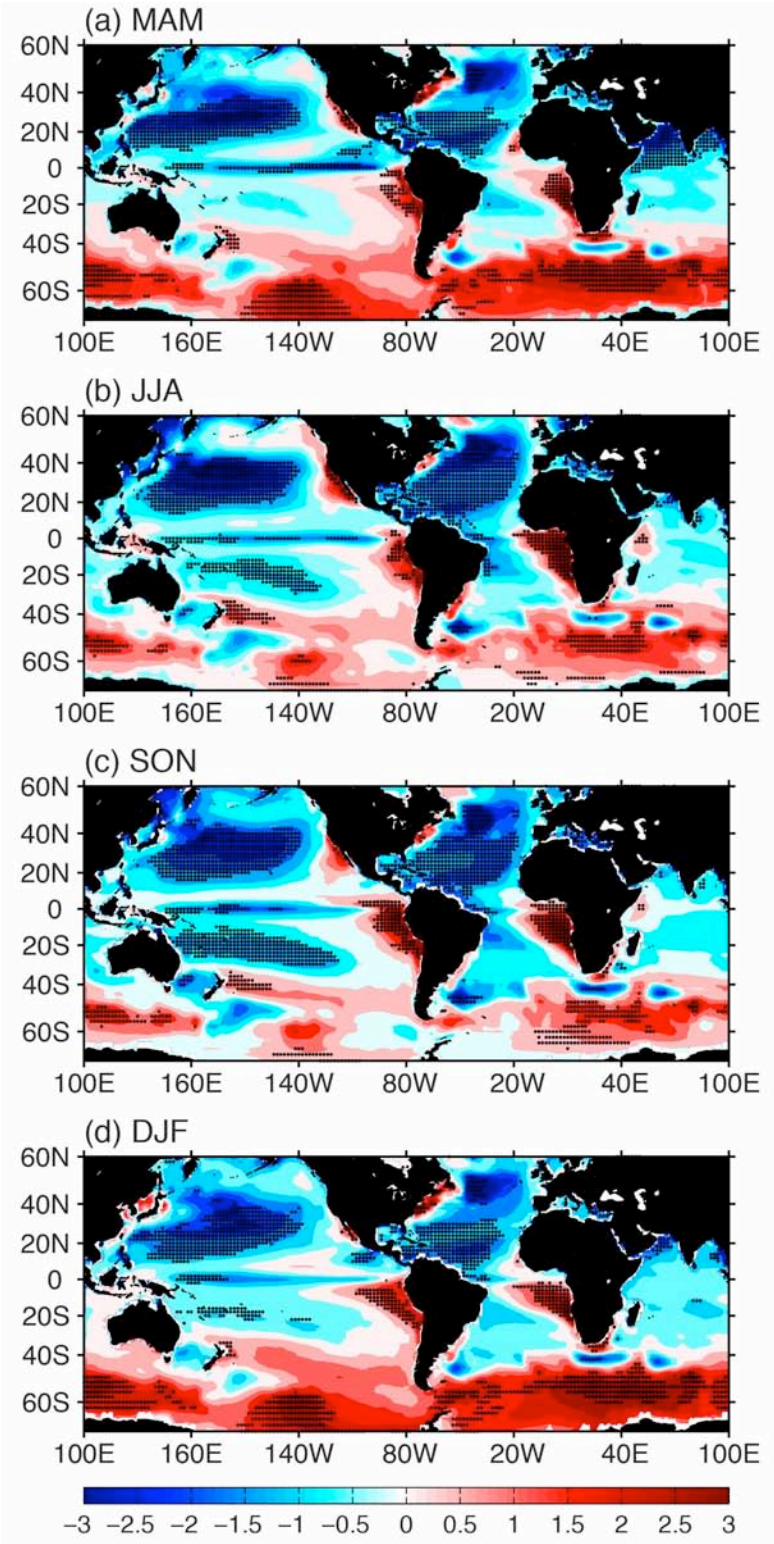

Figure S1. The seasonal variation of SST biases in 22 climate models. Shown are the SST bias during the boreal (a) spring (March-May, MAM), (b) summer (June-August, JJA), (c) fall (September-November, SON), and winter (December-February, DJF). The bias is calculated as the SST difference between simulated SST and observed ERSST. The dots denote where at least 18 of 22 models (i.e., 82%) have the same sign in the SST bias.

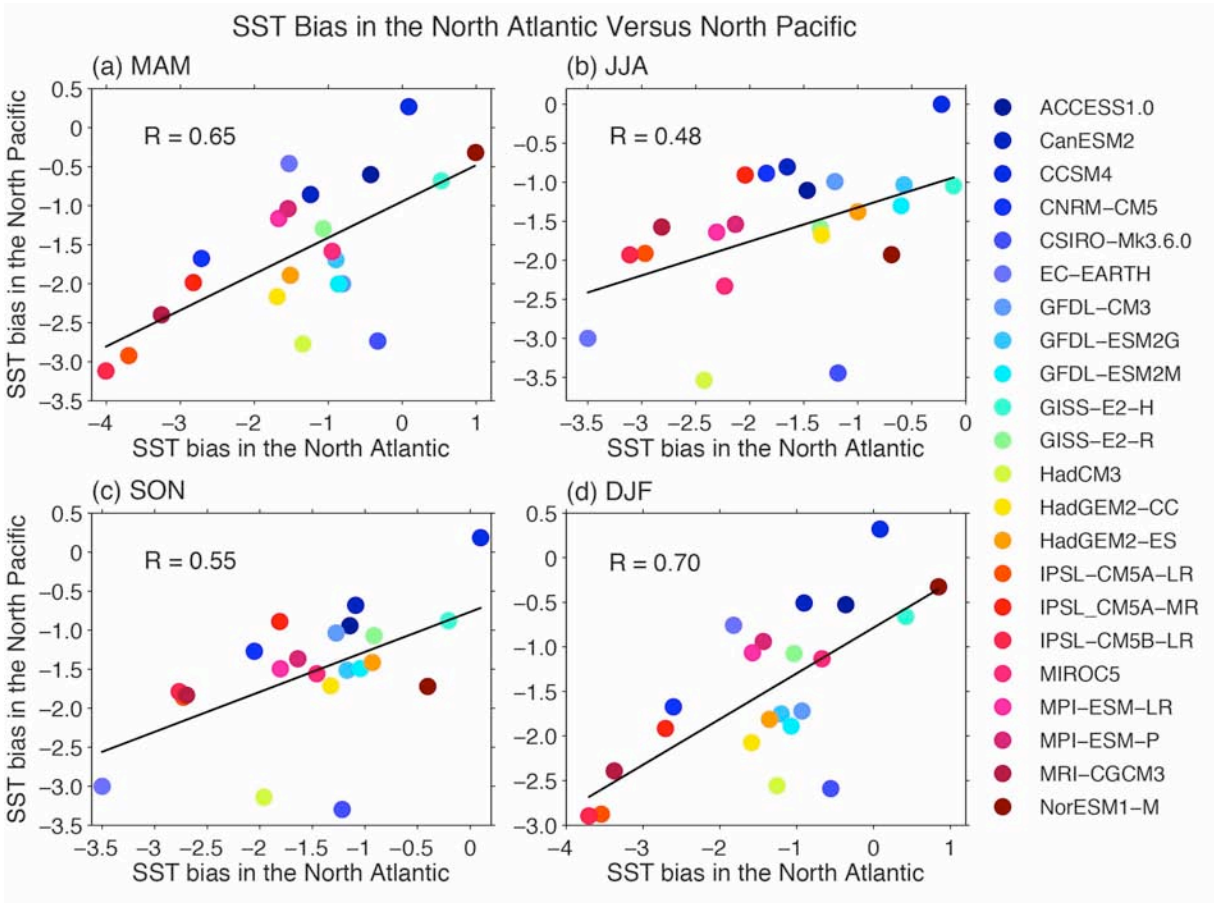

Figure S2. Relationship between the SST biases in the North Atlantic and North Pacific. Shown are scatterplots of the SST biases in the North Pacific versus North Atlantic during the boreal (a) spring (March-May, MAM), (b) summer (June-August, JJA), (c) fall (September-November, SON), and winter (December-February, DJF). The inter-model correlation R is shown in the left-upper side of each panel.

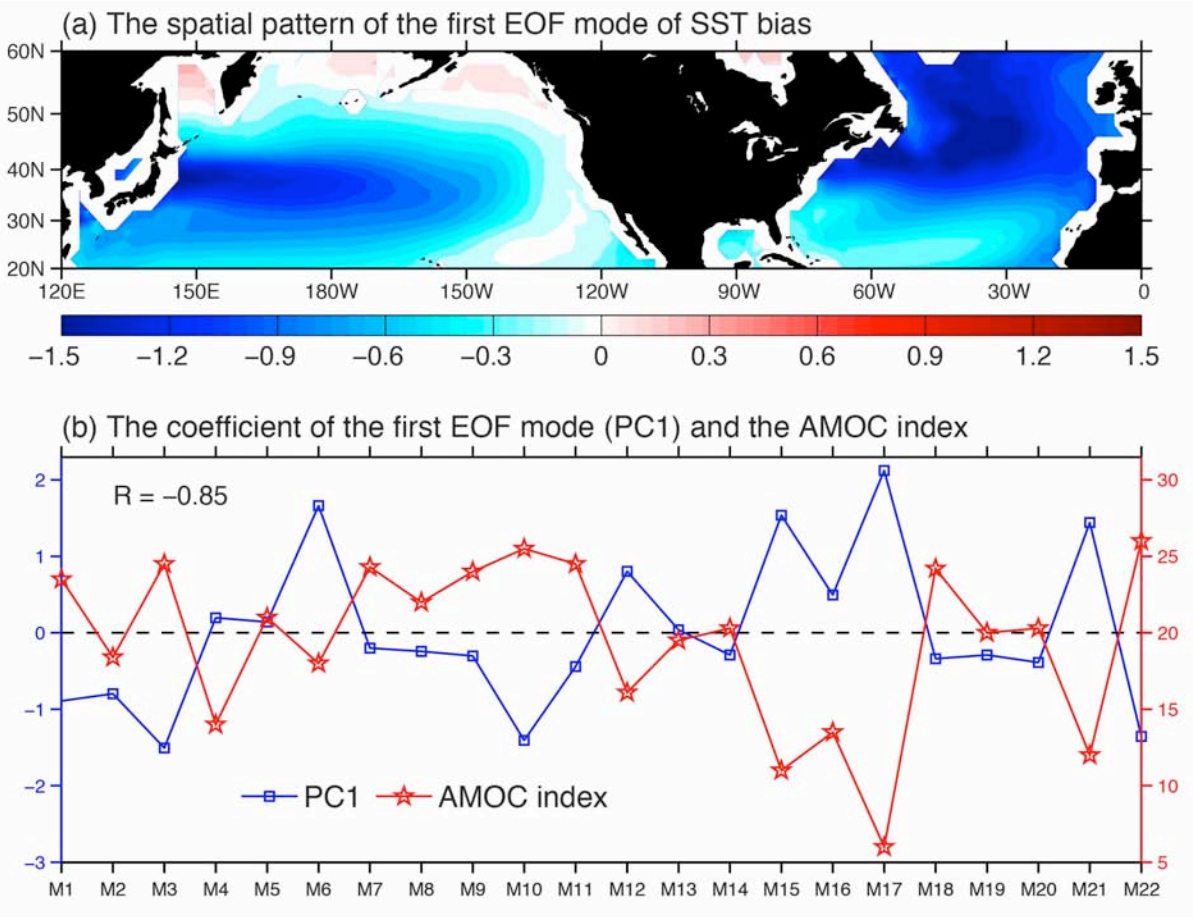

Figure S3. Inter-model EOF analysis of SST bias in the North Atlantic and North Pacific and the AMOC. Shown are (a) the first EOF mode spatial pattern of the SST bias in the Northern Hemisphere (20°N-60°N, 120°E-0°), and (b) PC1 of the first EOF mode and the AMOC index. The inter-model EOF analysis is performed by using different climate models as the time dimension. The x-axis in (b) represents different models (Supplementary Table S1). The first EOF mode accounts for 37% of the total variance. The second mode (accounting for 14% of the total variance) and higher modes do not correlate with the AMOC index (not shown).

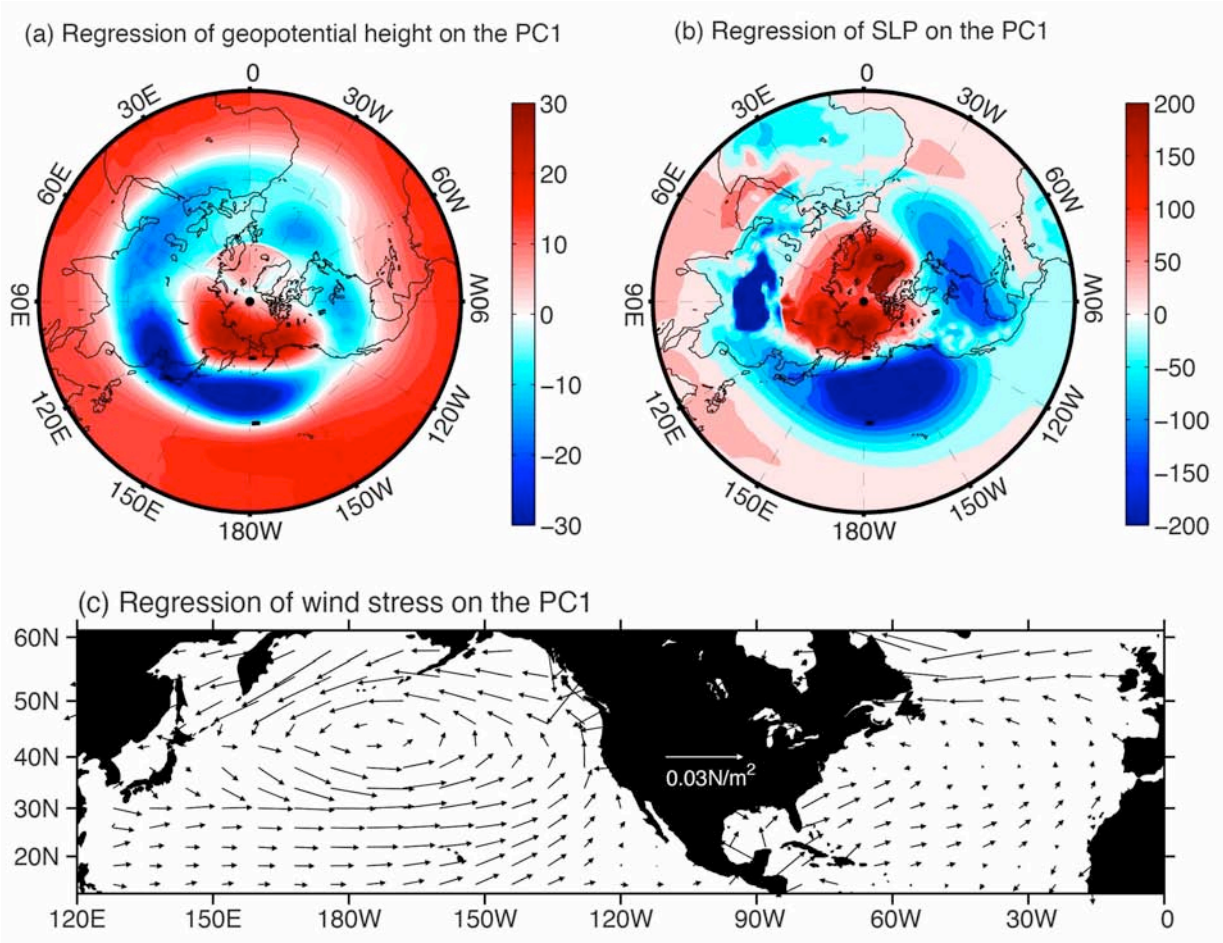

Figure S4. Regressed maps onto the first EOF mode. Shown are regressions of the (a) geopotential height (m) at 200 hPa, (b) sea level pressure (Pa), and (c) surface wind stress (N/m^2) onto PC1 of the first EOF mode of the SST bias.

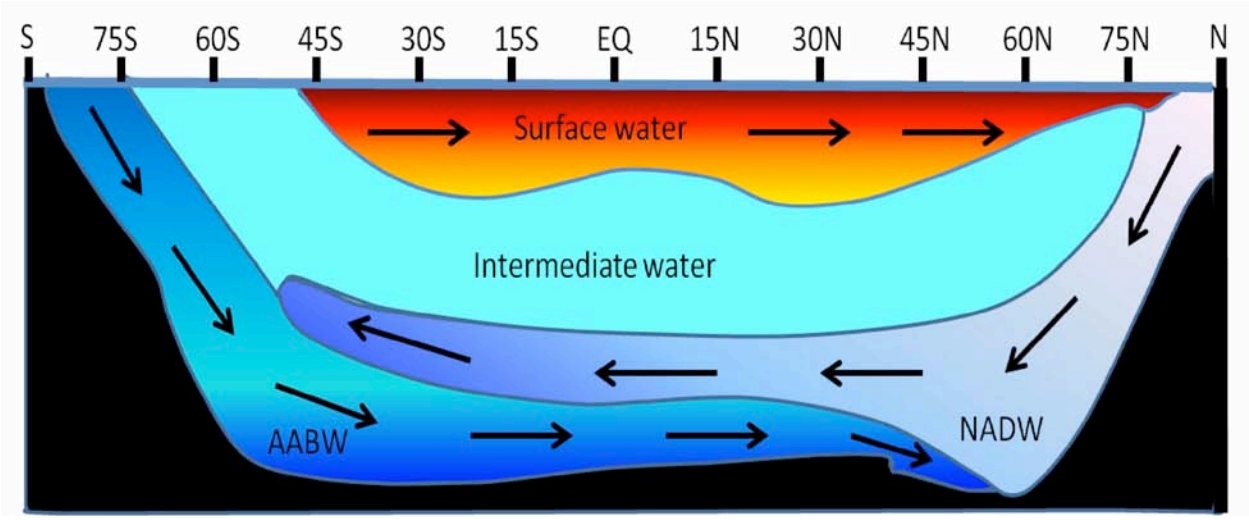

Figure S5. Schematic representing a zonally averaged picture of the Atlantic Ocean. The GMOC or AMOC consists of the upper and lower circulation cells: the North Atlantic Deep Water (NADW) cell and the Antarctic Bottom Water (AABW) cell. The color shading depicts the surface warm water, the intermediate water and the deep cold water.

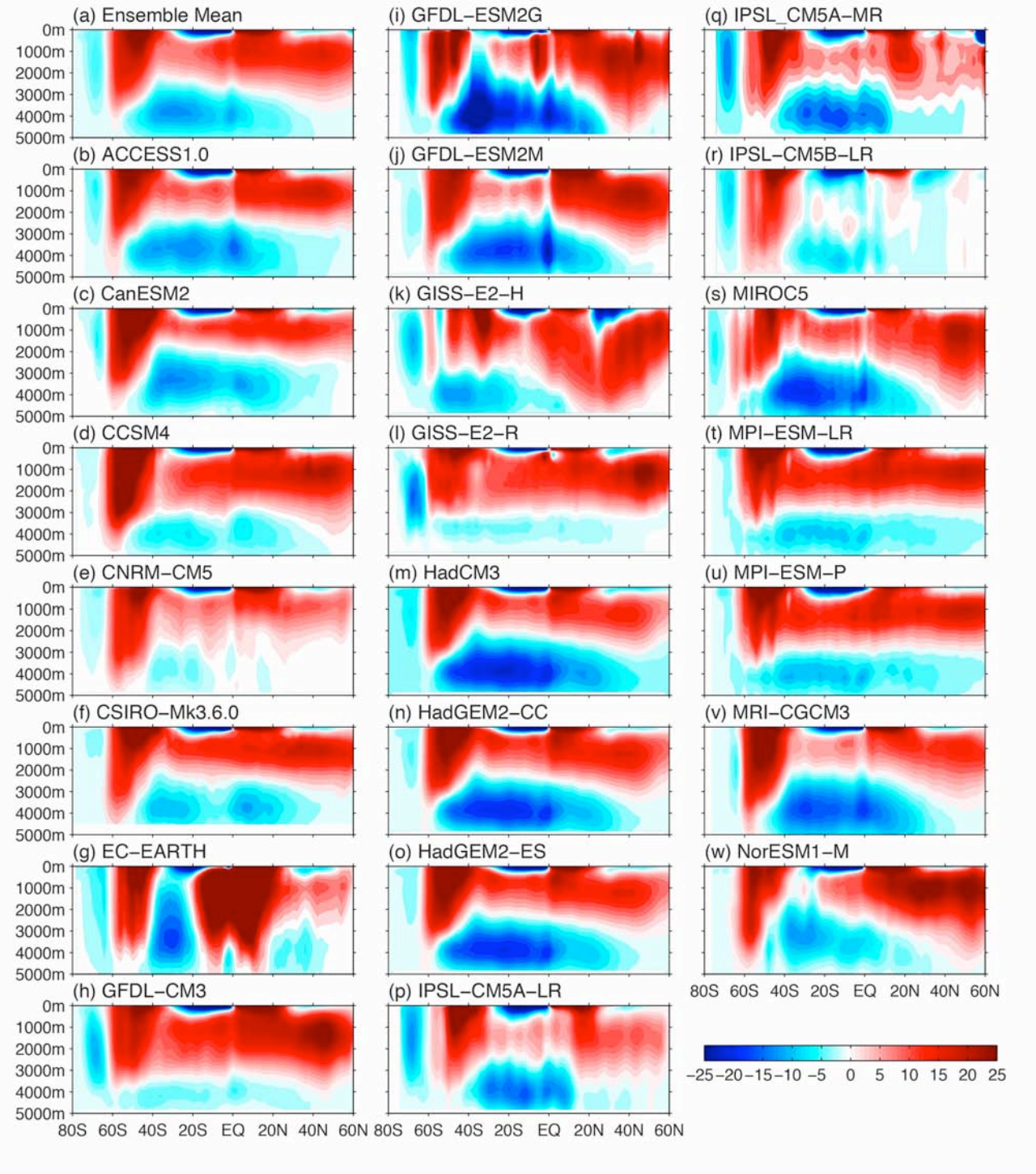

Figure S6. Long-term mean GMOC streamfunction (Sv) from 22 CMIP5 climate models.

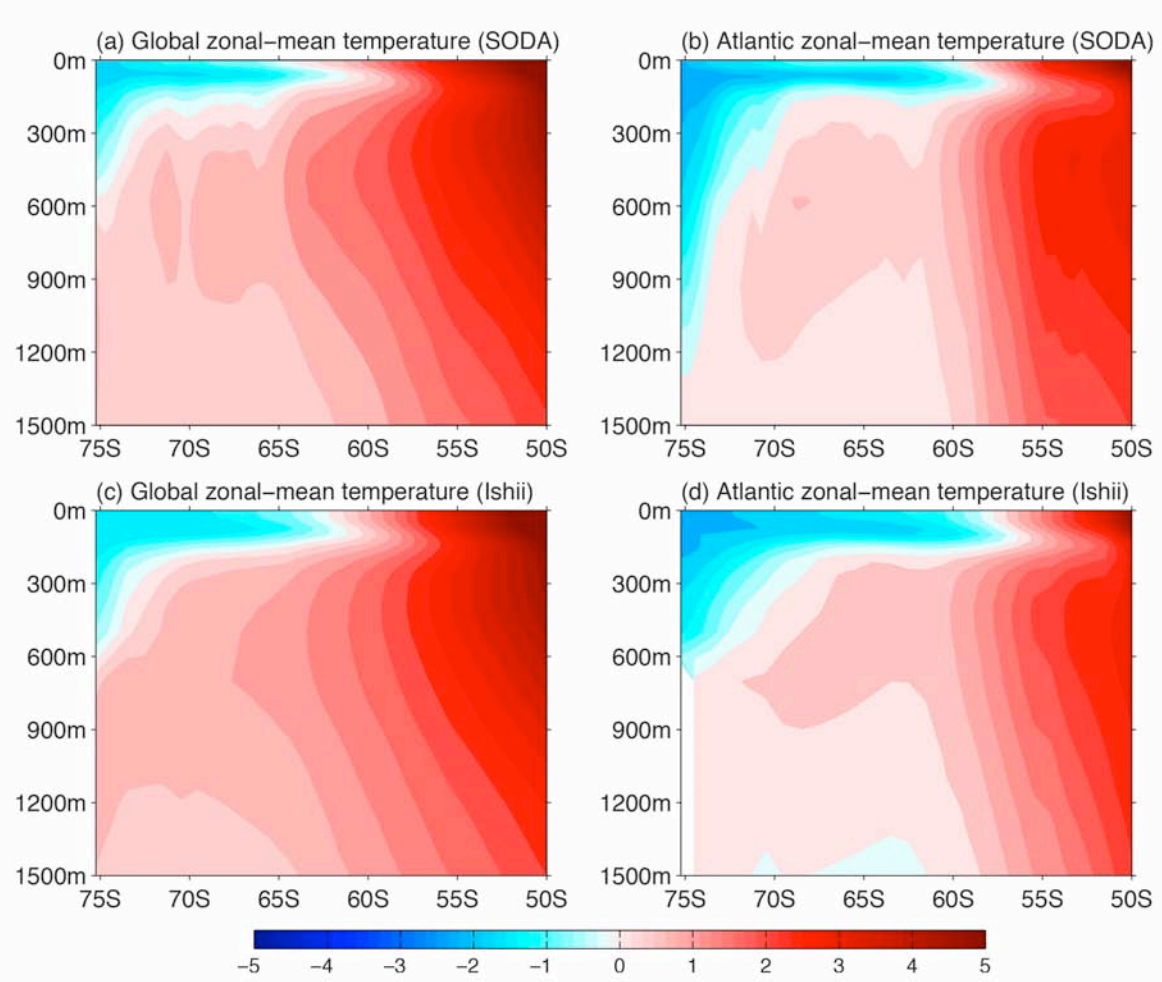

Figure S7. Vertical structure of long-term mean temperature in the SO. The top panels are the (a) global and (b) Atlantic (60°W-20°E) zonal-mean temperature (°C) from the SODA data. The bottom panels are the (c) global and (d) Atlantic (60°W-20°E) zonal-mean temperature (°C) from the Ishii data.

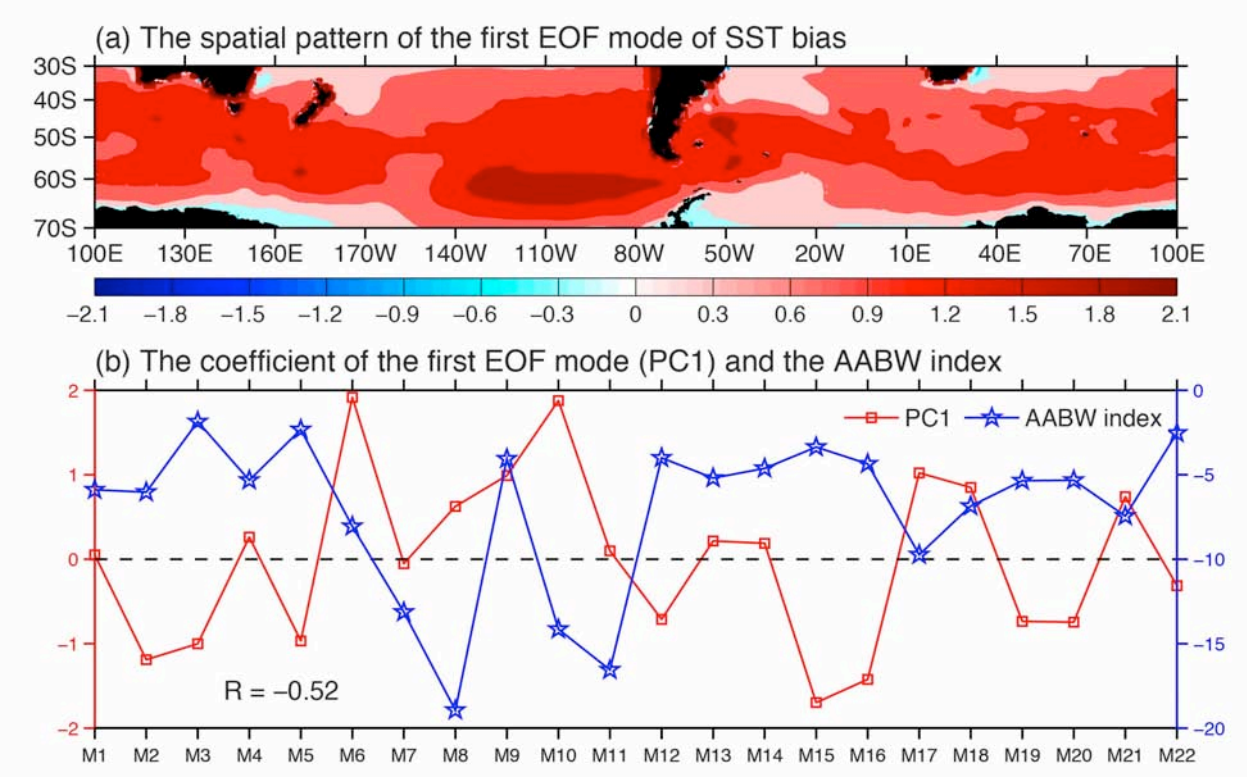

Figure S8. Inter-model EOF analysis of the SO SST bias and AABW. Shown are (a) the first EOF mode spatial pattern of the SST bias in the SO, and (b) PC1 of the first EOF mode and the AABW index. The inter-model EOF analysis is performed by using different models as the time dimension. The x-axis in (b) represents different models (Supplementary Table S1). The first EOF mode accounts for 69% of the total variance. The second mode (accounting for 8% of the total variance) and higher modes do not correlate with the AABW index (not shown).

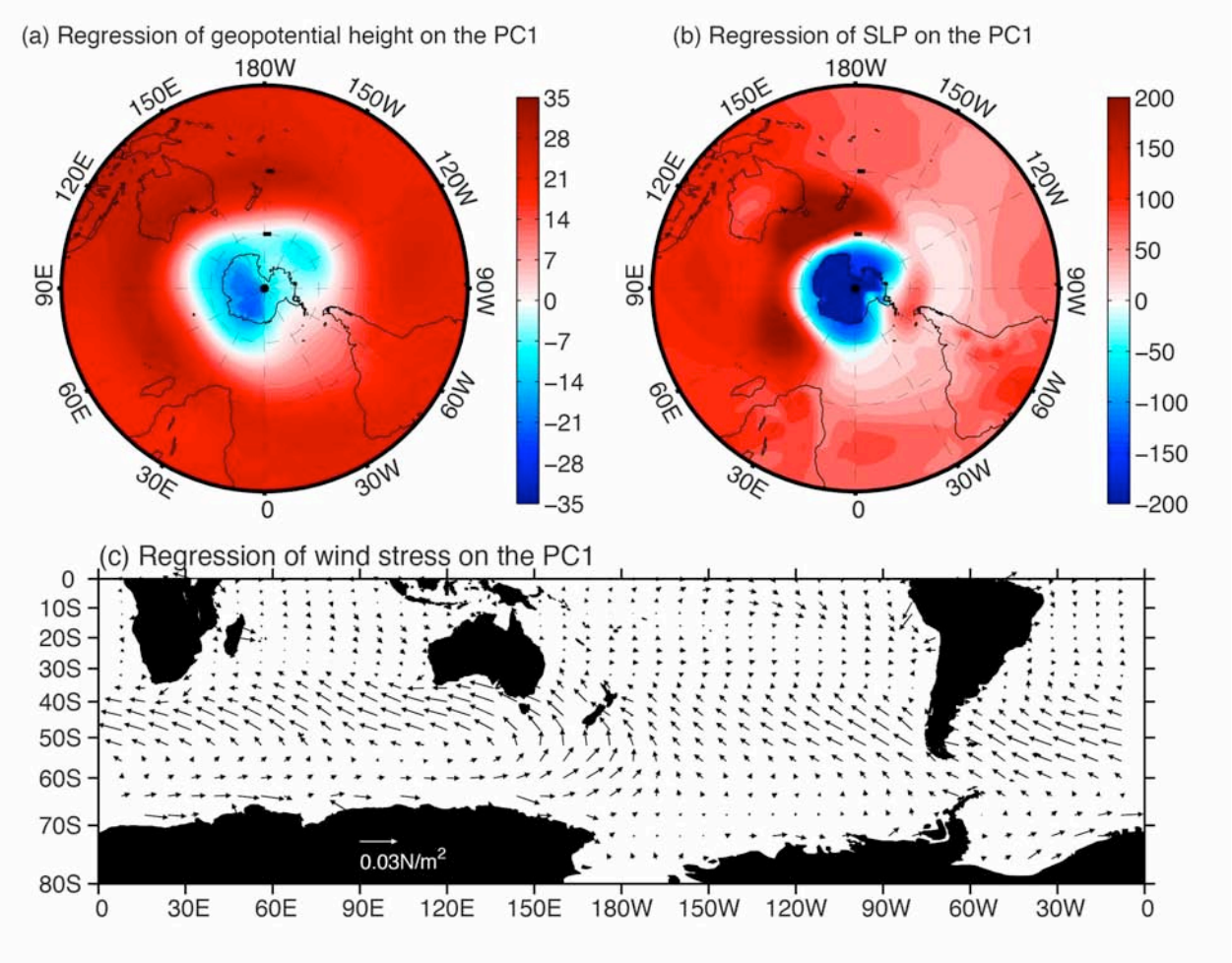

Figure S9. Regressed maps onto the first EOF mode of the SO SST bias. Shown are regressions of the (a) geopotential height (m) at 200 hPa, (b) sea level pressure (Pa), and (c) surface wind stress (N/m^2) onto PC1 of the first EOF mode of the SST bias in the SO.

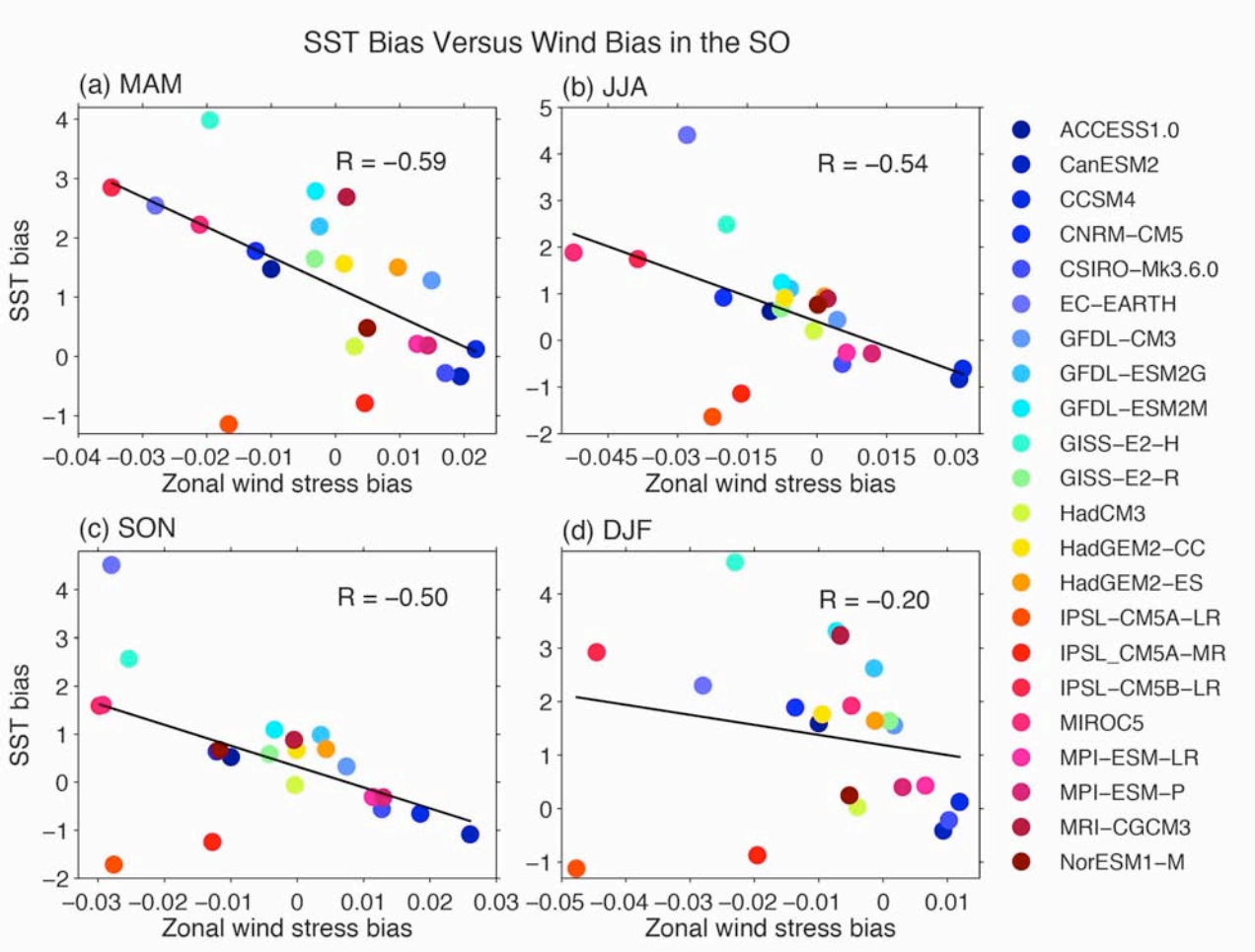

Figure S10. Relationships of SST and zonal wind biases in the SO. Shown are scatterplots of the SST bias versus the zonal wind stress bias in the SO during the boreal (a) spring (March-May, MAM), (b) summer (June-August, JJA), (c) fall (September-November, SON), and winter (December-February, DJF). The inter-model correlation R is shown in the right-upper side of each panel.

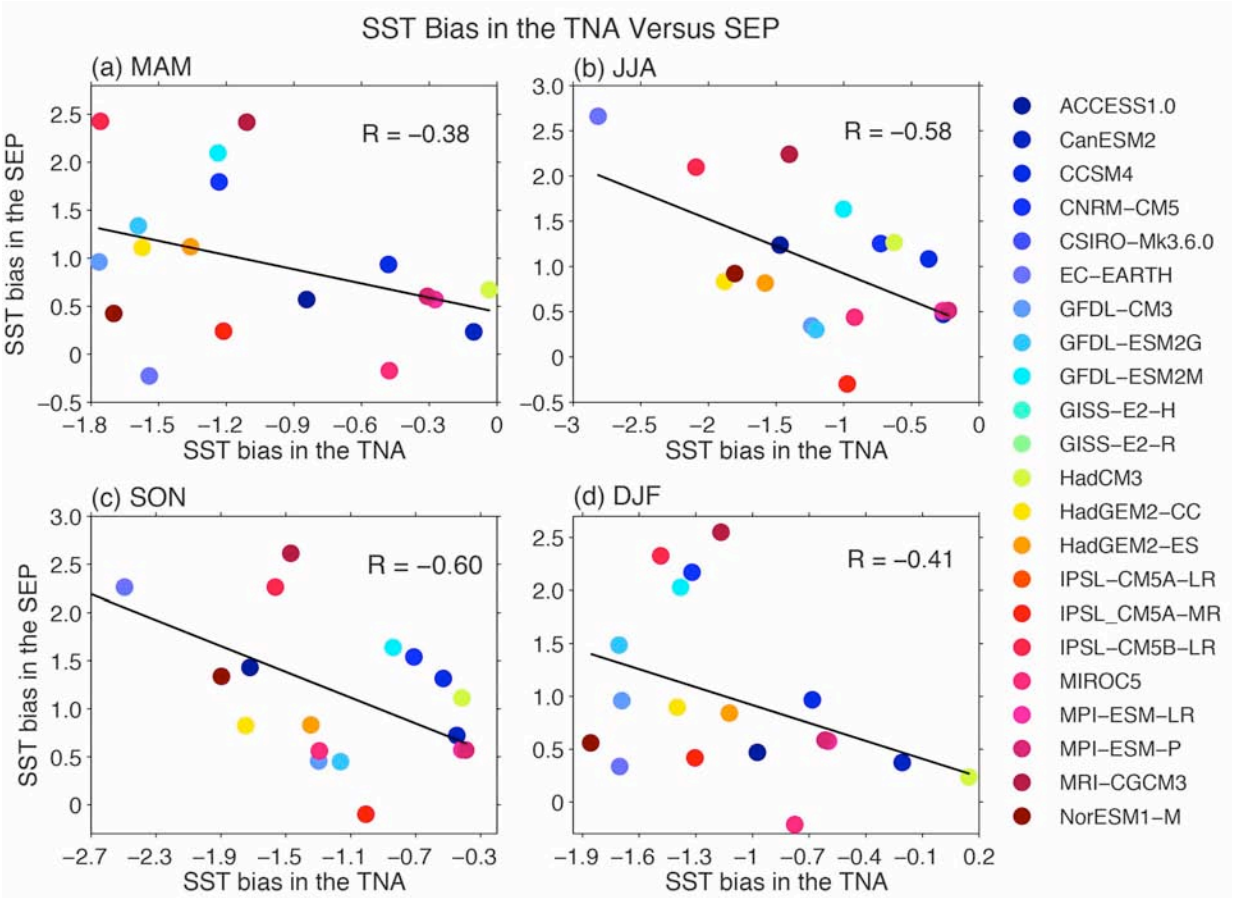

Figure S11. Relationship between SST biases in the tropical southeastern Pacific (SEP) and the tropical North Atlantic (TNA). Shown are scatterplots of the SST (°C) bias in the SEP versus the SST bias in the TNA during the boreal (a) spring (March-May, MAM), (b) summer (June-August, JJA), (c) fall (September-November, SON), and winter (December-February, DJF). The inter-model correlation R is shown in the right-upper side of each panel.

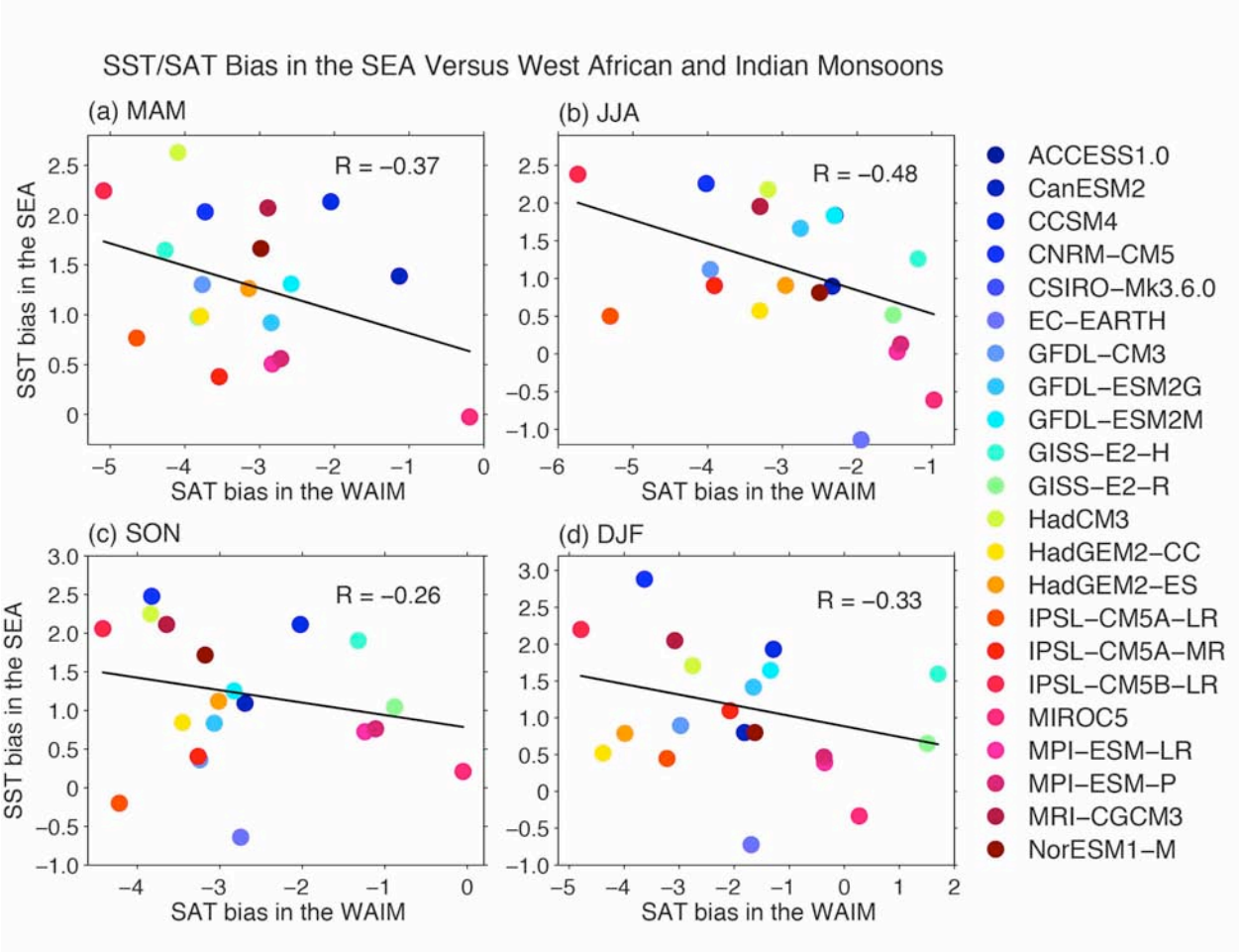

Figure S12. Relationship between SST bias in the tropical southeastern Atlantic (SEA) and surface air temperature (SAT) bias in the region of the West African and Indian monsoons (WAIM). Shown are scatterplots of the SST bias in the SEA versus the SAT bias in the WAIM during the boreal (a) spring (March-May, MAM), (b) summer (June-August, JJA), (c) fall (September-November, SON), and winter (December-February, DJF). The inter-model correlation R is shown in the right-upper side of each panel.